Energy Harvesting Eel

J.J. Allen[1] , A.H. Techet[1], R.M. Kelso[2] and A.J. Smits[1]

[1]Department of Mechanical and Aerospace Engineering
Princeton University, New Jersey, 08544, USA

[2]Department of Mechanical Engineering
Adelaide University, Adelaide, South Australia, 5005 AUSTRALIA

Abstract

Experiments were performed to investigate the possibility of using flexible piezoelectric membranes as power generation devices in the ocean. These membranes are excited by the von Kármán vortex street forming behind a bluff body. Experiments show a number of flow regimes, ranging from poorly coupled, where the membrane essentially acts as splitter plate and suppresses vortex shedding, to an optimally coupled state, where the membrane oscillates at the natural frequency of the undisturbed wake. The details of the interaction between the wake vortices and the membrane are studied using Particle Image Velocimetry and interpreted using topological concepts.

Introduction

To perform long endurance military missions, small, unattended sensors must generate and harvest power from their surroundings. Recent experiments of Allen & Smits [1], investigating the possibility of using piezoelectric polymers as power generation devices, have shown that a flexible membrane can be excited in a flag-like fashion by the von Kármán vortex street forming behind a bluff body. It is anticipated that 1 m^2 of membrane should be capable of producing 1 watt of power.

Flows behind bluff bodies in the Reynolds number range 10^3-10^5 are characterized by the formation of a vortex street of reasonably constant Strouhal number. The vortex streets in this range have a strongly three-dimensional character. Huerre & Monkewitz [2] provide a description and review the formation of the von Kármán vortex street in terms of being the result of a local absolute instability growing into a global linear instability and arguing that vortex street formation does not involve details of flow separation from the bluff body. A detailed description of the vortex formation process behind a flat plate is given in Perry & Steiner [5].

The behaviour of a flexible membrane, placed in the wake of a bluff body, has received little attention in the literature. The presence of a rigid splitter plate behind a bluff body can have dramatic effects in terms of reducing and/or suppressing vortex street formation, e.g. Roshko [3], and Gerrard [4]. The effect of splitter plates is relevant in the current study because in some flow configurations the membrane is stiff enough to act as a rigid splitter plate. However, if the membrane has small inertia and is flexible enough to respond rapidly to the unsteady pressure field set up by the vortex shedding, one may expect the membrane to oscillate with a wavelength and frequency similar to those observed in the unobstructed wake. This results in a coupled fluid/structure interaction.

Experiments

Four different membranes were tested in a water channel running at speeds of 0.05 to 0.8m/s. Two different bluff body widths were used, 3.81cm and 5.08cm, resulting in a Reynolds number range, $Re_D = U_\infty D / \nu$, of $5 \times 10^3 - 4 \times 10^4$. The aspect ratios of the bluff bodies were 6 and 10 respectively.
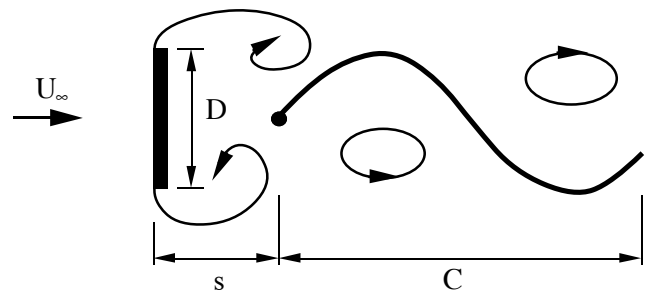

Figure 1. Geometry of an oscillating membrane placed behind a flat plate in a free stream of strength U_∞.

The diagram in figure 1 shows the important experimental parameters involved in describing the behavior of the undulating eel. D is the width of the bluff body, s is the distance downstream of the bluff body that the head of the eel is placed and U_∞ is the free stream velocity. The physical properties of the eel are described in terms of its stiffness E, length L, thickness h, width W, second moment of area I and mass per unit length ρ_{eel}. The streamwise extent of the eel in operation is defined by the chord length C. Figure 1 also shows an interpretation of the vortical structures forming over the membrane. Experiments were conducted in a recirculating water channel 47.5cm wide and 12.7cm deep. The ratio of gap width s to bluff body size D was equal to unity in the experiments.

Particle image velocimetry (PIV) and flow visualization using fluorescent dye were both performed to obtain information about the nature of the flow around the membrane. The PIV system consisted of an externally triggered Cohu 6600-3000 series full frame transfer camera, 659 x 496 pixels, with 10-bit resolution, working in conjunction with an Argon-Ion laser. The camera was operated in asynchronous frame transfer mode, allowing image pairs to be captured with time delays as small as 0.5 ms, and at image pair acquisition rates up to 30Hz. Each pixel corresponded to 0.2 x 0.2 mm in the flow. The captured data were cross-correlated using in-house PIV software, applying 32 x 32 pixel interrogation windows with 50% overlap. Typical particle shifts between image pairs were 12 pixels. The flow was seeded with 5µm silver-coated hollow spheres from PQ Corporation. The images presented in figures 6 and 7 are constructed from two offset images obtained at the same phase of the vortex shedding cycle.

Results

In the Reynolds number range 5,000-50,000 the Strouhal number, $St_n = f_n D / U_\infty$, behind the 3.81cm bluff body was equal to 0.15 and for the 5.08cm bluff body it was 0.16. This slight variation is a result of the differences in tunnel blockage. St_n was essentially invariant over the range of Reynolds numbers being investigated Four membranes were tested The first two were

45.7*cm* (18") and 60.9*cm* (24") long and made from Polyvinyline Di-Fluoride (PVDF), which is a piezoelectric polymer that generates a voltage potential when strained. A third membrane was constructed from a polyurethane (PU) core, with two thin outer layers of PVDF. The fourth membrane was made from plastic shim stock, selected so as to have similar natural frequencies to the PVDF membrane but with a much smaller mass per unit length. The width of all membranes, W, was 0.0762m. The dimensions and properties of the membranes are listed in table 1. The term EI/ρ_{eel} represents the effective stiffness of the membrane in response to bending. Its value was determined directly from a static deflection test. This term is similar to the natural frequency of a spring/mass system.

Material	Thickness t(mm)	Length (m)	Mass (g)	EI/ρ_{eel} (m⁴sec⁻²)	L/D
18" PVDF	0.7	0.457	38g	0.0028	12, 9
24" PVDF	0.7	0.076	53g	0.0028	18, 12
18" PU	0.6	0.457	34g	0.00062	12
18" Shim	0.1	0.457	7g	0.0021	12

Table 1. Properties of membranes tested. All membranes were 0.0762 m wide.

Figure 2 shows dye visualization images behind a 5.08cm bluff body with and without a membrane present at a Reynolds number based on plate width, Re_D, of 10,000. At this Reynolds number, the vortex shedding behind the plate, although coherent, is strongly turbulent and three-dimensional. In figure 2(b) the membrane is shown executing large forced oscillations and the vortical structures are highlighted. The spacing of vortical structures in both images is approximately 1.9D. Although the flow visualization images in figure 2(a) and (b) show a somewhat similar spacing of vortical structures, the overall topologies of the two flows must be different as the membrane acts as a barrier to prevent material communicating between the separating shear layers.
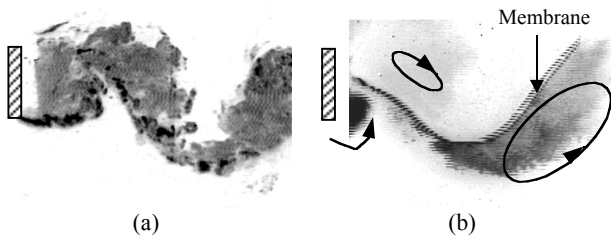

(a)   (b)

Figure 2. (a) Formation of a von Kármán vortex street without the membrane, and (b) the formation of coherent structures along a membrane in the wake of a bluff body.

To assess the behavior of the membranes, measurements were made of the frequency of oscillation. Figure 3 shows the responses of the eels tested, plotted with respect to their non-dimensional frequency, $St_{eel} = f_{eel}D/U_\infty$ and for a range of Reynolds numbers, Re_D.
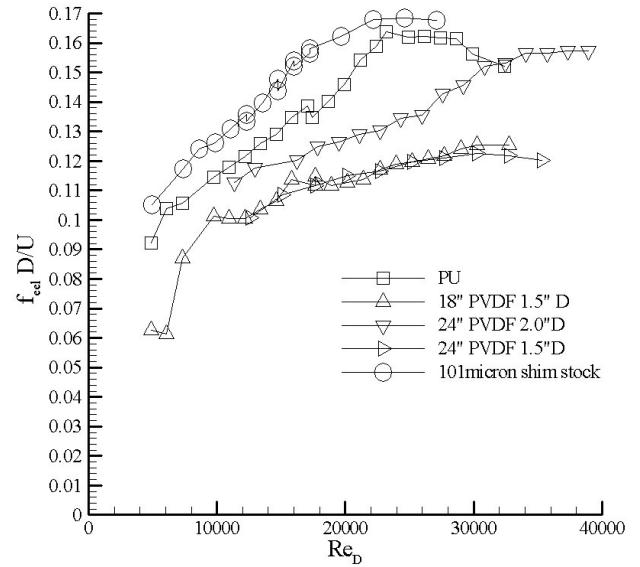

Figure 3   Scaling of St_{eel} number versus Re_D

At low Reynolds number, of order 2000, the amplitude of oscillation of all the membranes is small. St_{eel} is of the order 0.08. The oscillations in these cases are infrequent. In this mode the behavior of the eel can be interpreted as being similar to that of a rigid splitter plate. The membranes appear to be causing the separated shear layers from the bluff body to reattach on the eel surface and form a recirculation bubble, as shown in the dye visualization image in figure 4.
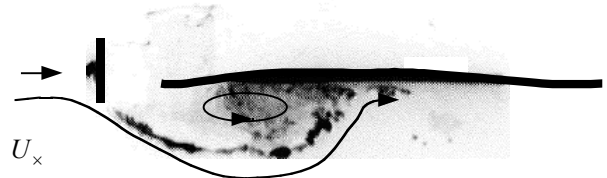

Figure 4. Flow visualization of the PU membrane at Re_D = 1,000 and D = 3.81cm.

As the Reynolds number increases, the membranes all show a tendency to oscillate periodically with a fairly constant Strouhal number at any given Re_D. However, although the membranes appear to be oscillating with a travelling waveform, they are not well coupled to the flow, as indicated by the fairly low value of $St_{eel} \approx 0.06 - 0.11$, indicating that the membrane exerts a damping effect on the flow. As the Reynolds number is further increased the membrane oscillations gradually increase in amplitude. This results in a decrease in wavelength of oscillation and a decrease in chord length of the eel. As this occurs there is also a trend for the non-dimensional frequency of the membrane St_{eel} to approach the natural Strouhal number, St_n, of the bluff body. This indicates that the membrane is well coupled to the flow. The wavelength of the membrane shortens to a point where it appears that it closely resembles the spacing of the coherent structures in the wake of a plate without a membrane being present, as shown in the flow visualization image in figure 5. The amplitude of oscillation of the membrane in figure 5 appears to be similar to or larger than the width of the wake in when the
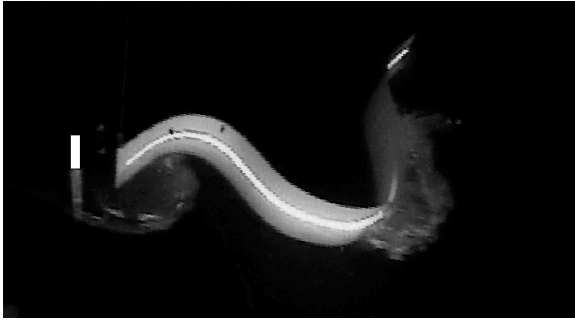
Figure 5. Membrane oscillation Re$_D$=20,000. The free stream flow is from left-to-right.

When $St_{eel} \approx 0.16$ was reached for each of the membranes the amplitude of oscillation remained relatively constant and a linear increase of oscillation frequency occurred with linear increase of flow speed. When the eel reaches the optimal coupling condition, $St_{eel} \approx 0.16$, its effective wavelength is constant. This implies that the phase speed of structures convecting along the membrane surface is approximately constant for a fixed flow velocity, regardless of the ability of the eel to couple to the flow. The phase speed is defined as $U_{phase} = \lambda f_{eel}$. The various data sets all show that as the Reynolds number increases the trend of the membrane behavior is towards optimal flow coupling, defined as $f_{eel}D/U_\infty \approx 0.16$, at different rates when scaled with respect to Reynolds number. This can be explained by the fact that the Reynolds number does not take into account any material properties of the eel, which obviously have a significant effect on the membrane response. An important aspect of the above data is that the frequency responses of the 60.9cm (24") and 45.7cm (18") membranes behind the $3.81cm$ plate are identical, suggesting that the membrane response does not depend critically on the length of the membrane, at least for the relatively large *L/D* ratios considered. The 60.9cm (24") membrane displays a marked improvement in response behind the $5.08cm$ bluff body compared to the 45.7cm (18") membrane placed behind the $3.81cm$ bluff body, indicating a significant response sensitivity to the bluff body size. The shim stock membrane, which has almost the same natural frequency as the 45.7cm PVDF membrane displays far superior coupling to the flow, suggesting that inertial or internal damping effects are important factors in a description of the ability of a membrane to couple to the flow. All the data sets show a levelling out of the non-dimensional frequency, indicating that the oscillation appears to have an upper bound of frequency as determined by the bluff body size and flow speed. This would also indicate that the observed phenomenon is not self-excited oscillation of the eel itself, but critically dependent on the presence and size of the bluff body.

Figure 6 shows the streamline pattern developing around the membrane during one oscillation cycle, obtained from PIV measurements. The region shown represents approximately three quarters of the membrane chord length. Figure 6 (a) shows the presence of two coherent vortical structures, **A** and **B**, on the membrane. Vortex **A** is starting to convect along the underside of the membrane while vortex **B** is beginning to impinge on the top surface of the membrane. Both structures show that reversed flow exists on the surface of the membrane close to the pivot point, indicating that secondary vorticity, of opposite sign to the impinging structures, is being generated on the membrane surface under these structures. Figure 6 (b) shows that the membrane appears to be deforming significantly in response to the

velocity relative to the stationary observer (see below). In figure 6(c) vortex **B** appears to be significantly deforming in response to the membrane, that is now moving upwards as the result of a newly impinging vortex, vortex **C**. An interesting feature of figure 6(c) is the appearance of a saddle point in the flow below the core of vortex **B**, indicating that two streamlines terminating at the eel surface have joined and bifurcated away from the surface. Figure 6(d), the final phase in the shedding cycle, shows vortex **C** beginning to convect along the surface and the appearance of a saddle point in the free stream separating the like signed vortical structures, vortex **B** and **D**. There is reversed flow between this saddle point and the membrane surface and hence a transport of material upstream towards vortex **D**. This transport of material has also been observed in flow visualization experiments.
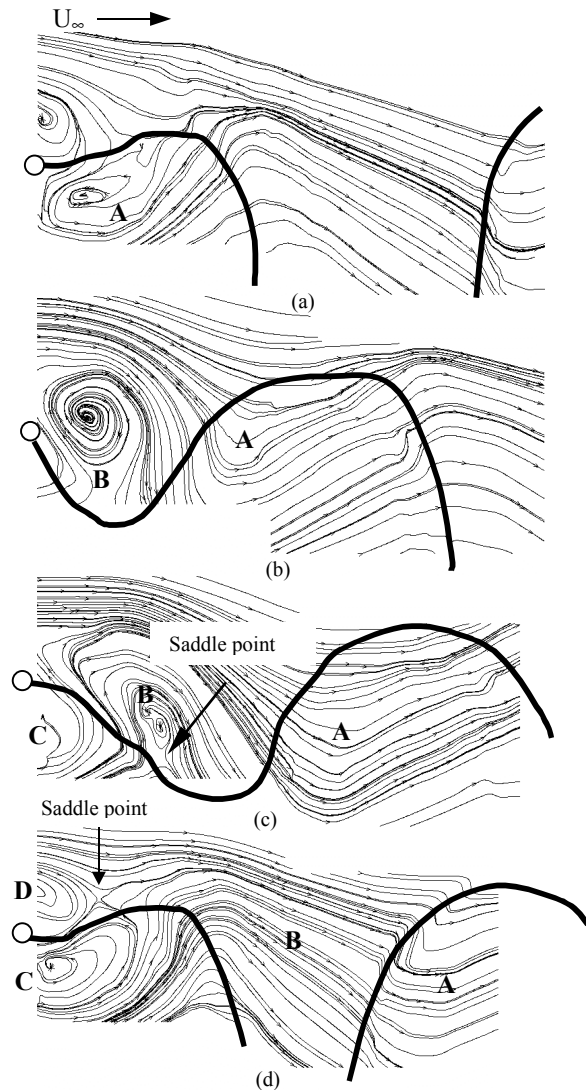

Figure 6 (a)-(d)   Streamline patterns showing four stages within the vortex shedding cycle, viewed from a stationary frame of reference.   The shape of the eel has been overlaid to aid interpretation.

Figure 7 shows the streamline pattern of figure 6(d) when a bias velocity of 0.65 U_∞ has been applied. This velocity bias results in the membrane appearing as a streamline in the flow and also shows the presence of structures along the length of the membrane for the full field of view.   This streamline pattern agrees well with the flow visualization results in terms of

surface between vortices B and D. Note also that vortex B is identifiable only by distorted streamlines in figure 6(d) – there is no evidence of circulation. This is a result of the high convention velocity of vortex B relative to the stationary observer. However, in figure 7, the flow pattern is presented as seen by an observer moving with a velocity close to the convection velocity of the shed vortices. In this reference frame vortex B is recognisable as a vortex. The same argument can be applied to all vortices once shed from the bluff body, including vortex A which appears on the right side of figure 7.
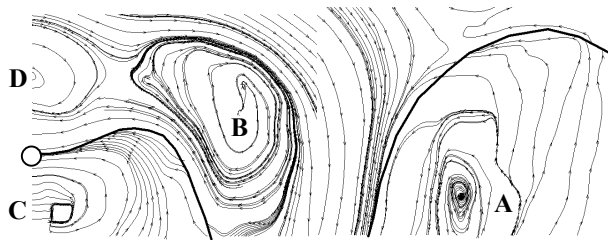

Figure 7. Streamline pattern as seen by an observer moving downstream with bias velocity of $0.65U_\infty$.
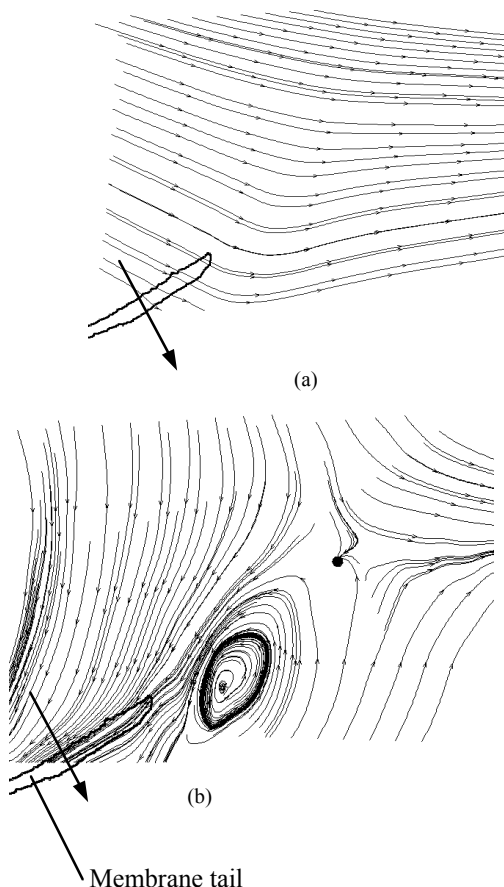

(a)

(b)

Membrane tail

Figure 8. Streamline pattern around membrane tail; (a) stationary frame of reference and (b) moving with a bias velocity of $0.9U_\infty$.

Figure 8 shows a streamline pattern in the region of the tail of the membrane in (a) a stationary frame of reference, and (b) when a bias velocity of $0.9\,U_\infty$ has been applied. In figure 8(b) the presence of a coherent structure being shed from the tip of the membrane can be clearly seen. However its strength is weak, as indicated by the bias velocity that has been applied. The apparently low strength of the shed vortex may be a result of the interaction between the bluff body vortices and the boundary layer vorticity of the opposite sense that is generated at the surface of the membrane.

Conclusions

The response of a flexible membrane or "eel" to external forcing due to the vortex shedding downstream from a bluff body has been examined using dye visualization, frequency measurements and PIV. The data show that the membranes are able to lock in to the bluff body shedding. Lock-in occurs when the membranes oscillate at the same frequency as the undisturbed wake behind the bluff body. When the membrane reaches this condition its wavelength and amplitude are also similar to those of the undisturbed von Kármán vortex street. PIV data indicate the presence of vortical structures convecting along the length of the membrane at a phase speed similar to the speed of the travelling wave along the membrane. These structures correspond to the alternating vortices that are formed and shed from the edges of the bluff body, as indicated by the flow visualization results. The strength of the coherent structures appears to be highly diminished by the time they are shed into the wake of the membrane. It is proposed that this is caused by the interaction of the impinging structures with boundary layer vorticity formed on the membrane surface.

References

[1] Allen, J. J. & Smits, A. J., Energy Harvesting Eel, *Journal of Fluids and Structures,* **15**, 2001, 629-640.
[2] Huerre, P. & Monkewitz, P. A., Local and global instabilities in spatially developing flows. *Annual Review of Fluid Mechanics,* **22**, 1990, 473-537.
[3] Roshko, A., On the drag and shedding frequency of two-dimensional bluff bodies. *NACATN* no. 3169, 1954.
[4] Gerrard, J. H., The mechanics of the formation region of vortices behind bluff bodies. *Journal of .Fluid Mechanics,* **25**, 1966, 401-413.
[5] Perry, A. E. & Steiner, T. R., Large-scale vortex structures in turbulent wakes behind bluff bodies. Part 1. Vortex formation process. *Journal of .Fluid Mechanics* **174**, 1987, 233-270.

Acknowledgments